HHS Public Access

Author manuscript

Acta Biomater. Author manuscript; available in PMC 2018 August 01.

Published in final edited form as:

Acta Biomater. 2017 August ; 58: 386–398. doi:10.1016/j.actbio.2017.06.004.

Highly efficient delivery of potent anticancer iminoquinone derivative by multilayer hydrogel cubes

Bing Xue[1,§], **Wei Wang**[2,3,§], **Jiang-Jiang Qin**[2], **Bhavitavya Nijampatnam**[1], **Srinivasan Murugesan**[1], **Veronika Kozlovskaya**[1], **Ruiwen Zhang**[2,3,*], **Sadanandan E. Velu**[1,5,*], and **Eugenia Kharlampieva**[1,4,*]

[1]Department of Chemistry, University of Alabama at Birmingham, Birmingham, AL, 35294, United States

[2]Department of Pharmaceutical Sciences, School of Pharmacy, Texas Tech University Health Sciences Center, Amarillo, TX, 79106, United States

[3]Cancer Biology Center, School of Pharmacy, Texas Tech University Health Sciences Center, Amarillo, TX, 79106, United States

[4]Center of Nanoscale Materials and Biointegration, University of Alabama at Birmingham, Birmingham, AL, 35294, United States

[5]Comprehensive Cancer Center, University of Alabama at Birmingham, Birmingham, AL 35294-3300, United States

Abstract

We report a novel delivery platform for a highly potent anticancer drug, 7-(benzylamino)-3,4-dihydro-pyrrolo[4,3,2-de]quinolin-8(1H)-one (BA-TPQ), using pH- and redox-sensitive poly(methacrylic acid) (PMAA) hydrogel cubes of micrometer size as the encapsulating matrix. The hydrogels are obtained upon cross-linking PMAA with cystamine in PMAA/poly(N-vinylpyrrolidone) multilayers assembled within mesoporous sacrificial templates. The BA-TPQ-loaded hydrogels maintain their cubical shape and pH-sensitivity after lyophilization, which is advantageous for long-term storage. Conversely, the particles degrade in vitro in the presence of glutathione (5 mM) providing 80% drug release within 24 h. Encapsulating BA-TPQ into hydrogels significantly increases its transport via Caco-2 cell monolayers used as a model for oral delivery where the apparent permeability of BA-TPQ-hydrogel cubes was ~2-fold higher than that of BA-TPQ. BA-TPQ-hydrogel cubes exhibit better anticancer activity against HepG2 (IC_{50}=0.52 μg/mL) and Huh7 (IC_{50}=0.29 μg/mL) hepatoma cells with a 40% decrease in the IC_{50} compared

[*]The corresponding authors with shared seniority: Prof. Eugenia Kharlampieva, Department of Chemistry, University of Alabama at Birmingham, 901 14th Street South, CHEM291, Birmingham, AL 35294, USA. ekharlam@uab.edu. Telephone: +1-205-934-0974. Prof. Sadanandan E. Velu, Department of Chemistry, University of Alabama at Birmingham, 901 14th Street South, CHEM280, Birmingham, AL 35294, USA. svelu@uab.edu. Telephone: +1-205-975-2478. Prof. Ruiwen Zhang, Department of Pharmaceutical Sciences, School of Pharmacy, Texas Tech University Health Sciences Center, 1300 Coulter Drive, Amarillo, TX, 79106, USA. ruiwen.zhang@ttuhsc.edu. Telephone: +1-806-414-9248.

[§]The authors equally contributed to this work.

to the non-encapsulated drug. Remarkably, non-malignant liver cells have a lower sensitivity to BA-TPQ-hydrogel cubes with 2-fold increased IC_{50} values compared to those of cancer cells. In addition, encapsulating BA-TPQ in the hydrogels amplifies the potency of the drug via down-regulation of MDM2 oncogenic protein and upregulation of p53 (a tumor suppressor) and p21 (cell proliferation suppressor) expression in HepG2 liver cancer cells. Moreover, enhanced inhibition of MDM2 protein expression by BA-TPQ-hydrogel cubes is independent of p53-status in Huh7 cells. This drug delivery platform of non-spherical shape provides a facile method for encapsulation of hydrophobic drugs and can facilitate the enhanced efficacy of BA-TPQ for liver cancer therapy.

Graphical Abstract

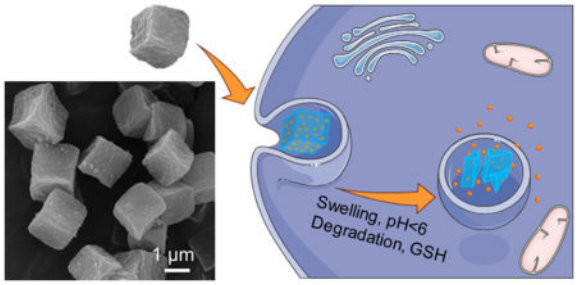

Keywords

Cubical hydrogel; multilayer hydrogel; intracellular degradable; poly(methacrylic acid); hydrophobic drug; BA-TPQ; Hepatocellular carcinoma

1. Introduction

Hepatocellular carcinoma (HCC) is the third leading cause of cancer death worldwide with high morbidity and mortality [1,2]. Current therapies have been shown to delay the development and progression of HCC to a certain extent: sorafenib, the predominant drug used for HCC treatment, can prolong the median survival of HCC patients by three months [3]. However, there is an urgent need to develop novel curative compounds to improve the therapeutic outcomes for patients with advanced HCC. An iminoquinone derivative, 7-(benzylamino)-1,3,4,8-tetrahydropyrrolo[4,3,2-de]quinolin-8(1H)-one (BA-TPQ), the most potent among the analogs of natural makaluvamine compounds, exerts anticancer activity against various cancer cells (e.g. breast cancer and prostate cancer) through multiple mechanisms including the suppression of the MDM2 oncoprotein, modulation of ZAK-MKK4-JNK-TGFβ signaling cascade, and the induction of endoplasmic reticulum stress [4–8]. Importantly, the BA-TPQ inhibition of tumor growth through down-regulation of MDM2 expression is independent of p53 status, demonstrating a broader range of anti-tumor effect even for the p53 mutant cancer cell lines [7]. However, despite its high potency against a variety of human cancer cell lines including breast and prostate tumors [8,9], the application of BA-TPQ has been limited by its poor solubility and low bioavailability. In addition, undesirable toxicity was observed in mice after administering BA-TPQ (a formulation of dispersed BA-TPQ in a mixture of PEG400/ethanol/0.9% saline [8,9]. Recent investigations

identifying the potential sites of accumulation to elucidate the observed BA-TPQ toxicity have revealed a high accumulation of BA-TPQ in the lungs, kidneys, and spleen of the mice [10,11]. Thus, an active drug delivery system for BA-TPQ is needed to improve anticancer efficacy and minimize side effects.

To surmount the limitations of unshielded therapeutic agents including low water-solubility, non-specific biodistribution, poor membrane permeability, multi-drug resistance, and toxicity towards non-malignant cells including those of bone marrow and the digestive tract [12–15], a variety of drug delivery platforms have been explored to improve the safety and efficiency of anticancer drugs [16–19]. Amphiphilic assemblies, such as micelles, polymersomes, and liposomes are widely used for hydrophobic drug delivery relying on physical entrapment of therapeutics within the hydrophobic polymer segments. However, their applications have been limited due to their potential structural instability *in vivo* where rapid vehicle disassembly may occur below the critical micelle concentration in the bloodstream [20].

Hydrogel particles have captivated the attention of researchers owing to their appealing physio-chemical properties and excellent versatility [21]. Their hallmark characteristics include large surface areas for functionalization, highly porous interior networks for drug loading, and easy tailoring of their geometry and surface morphology [22–24]. In contrast to organic or inorganic nanoparticles, hydrogels are soft materials which have elastic moduli ranging from 0.1 kPa to 100 kPa mimicking the elasticities of living cells and tissues and can regulate their bioactivities *in vitro* and *in vivo* [25–27]. Unlike self-assembled polymer structures such as micelles and liposomes, hydrogels possess exceptional mechanical stability because of their cross-linked structure and can undergo dramatic dimensional changes in response to stimuli in surrounding media causing on-demand drug release [28,29]. In addition to studies focusing on injectable drug delivery systems, hydrogel particles have been explored as potential carriers for oral delivery because of their excellent biocompatibility and diverse variety of material compositions [21,30].

Unlike the commonly used emulsion polymerization and precipitation polymerization methods for the synthesis of polymeric drug carriers, layer-by-layer (LbL) assembly of polymers at surfaces allows nanoscale control over the composition, chemistry, material thickness, and mechanical and stimuli-responsive properties of the resultant polymeric particles [31–33]. The LbL technique benefits from a vast selection of materials, as the interactions holding the multilayers together range from ionic-pairing and H-bonding to covalent and/or hydrophobic interactions [34,35]. The shape and size of LbL hydrogels are controlled by the respective dimensions of the colloidal templates which are dissolved after deposition to yield the polymeric networks [36]. In the case of non-porous templates, LbL assembly leads to hydrogel capsules with an interior cavity and nanothin walls, while alternating deposition of polymers inside porous templates results in nano-porous particles of interconnected macromolecular networks [37–40]. In the spirit of this concept we have recently demonstrated the synthesis of temperature- and pH-responsive nano-porous hydrogel microcapsules [41–43] and microparticles [37,38] of cubical shape. The cubic poly(methacrylic acid) (PMAA) hydrogel microparticles in this study were produced by sequential LbL infiltration of PMAA and poly(N-vinylpyrrolidone) (PVPON) inside 2 μm

porous cubic templates [37,38]. After the sequential infiltration of (PMAA/PVPON) bilayers, the on-template assembly was cross-linked with ethylenediamine or cystamine using carbodiimide-assisted coupling.

While it is known that size, surface charge, and hydrogel rigidity control the cellular interactions of hydrogel particles, the shape of the hydrogel particle has also been found to have a strong impact on cellular interactions including intravascular and transvascular transport, the rate and percentage of cellular internalization, and biodistribution [44]. For instance, the internalization rate of PMAA multilayer hydrogel microcapsules by HeLa cancer cells decreased as the capsule aspect ratio increased when cylindrical shapes were used instead of spherical ones [45]. In contrast to spherical capsules, the cubical shape of soft capsules has been shown to be crucial for favorable interactions with endothelial HMVEC and 4T1, MDA-MB-231, and SUM159 breast cancer cells [46]. The cubical capsules exhibited highly increased internalization in the breast cancer cell lines, indicating the importance of their shape in the process of cellular uptake.

Although various drug delivery systems have been applied to deliver poorly water-soluble cancer curative agents (e.g. paclitaxel, 5-fluorouracil and curcumin), the vehicular transport of BA-TPQ by non-spherical polymeric carriers has yet to be reported. Stimuli-responsive microgels with tailored shape for hydrophobic drug delivery have also been underexplored, which is mainly attributed to: (1) The highly water-favoring nature of the network which limits the interaction between microgel and hydrophobic molecules; (2) The synthetic challenges associated with fabricating and maintaining the 3-dimensional structure of shaped submicron-sized hydrogels without compromising stimuli-responsiveness. In previous works, the applications of pH [37] and dual pH/redox [38] PMAA hydrogel particles of cubical shape for encapsulation of the hydrophilic drug doxorubicin have been demonstrated. Nevertheless, the capability of this type of hydrogel for the transport of hydrophobic remedies has not been investigated. In addition, the effect of utilizing hydrogel particles as drug carriers on the therapeutic activity of BA-TPQ against tumor cells is still unknown.

In this work, a facile method has been developed to encapsulate BA-TPQ within the network of cubic PMAA hydrogel microparticles for liver cancer treatment. The polymer network in the multilayer hydrogels is “packed” throughout the volume of the cubes, providing an enormous surface area and structural stability which facilitates encapsulation of the hydrophobic BA-TPQ. The structural stability, pH- and redox- responsiveness, and their effects on loading and release of BA-TPQ has also been investigated. The application of multilayer PMAA hydrogel cubes as drug carriers can improve the trans-epithelial transport efficacy and the anti-tumor activity of BA-TPQ, demonstrating a potent platform for hydrophobic drug delivery and cancer therapy.

2. Materials and Methods

2.1 Materials

Poly(methacrylic acid) (PMAA, average M_w 21800 g mol^{-1}), poly(N-vinylpyrrolidone) (PVPON, average M_w 58000 g mol^{-1}), poly(ethylenimine) (PEI, average M_w 25000 g

mol^{-1}), were purchased from Sigma-Aldrich. 1-Ethyl-3-(3-(dimethylamino)propyl)-carbodiimide hydrochloride (EDC) was obtained from Chem-Impex International. Monobasic sodium phosphate, hydrochloric acid, sodium hydroxide, L-glutathione reduced (GSH), ethylenediaminetetraacetic acid (EDTA) and methanol were from Fisher Scientific and used as received. Ultrapure deionized water with a resistivity of 18 MΩ cm was used in all experiments (Evoqua). The anti-human p53 (DO-1) antibody was from Santa Cruz Biotechnology, Inc. (Santa Cruz, CA, USA). The anti-human MDM2 (Ab-2) and p21 (Ab-1) antibodies were from EMD Chemicals, Inc. (Gibbstown, NJ, USA). The anti-human β-actin (AC-15) antibody was from Sigma (St. Louis, MO, USA). The goat anti-mouse IgG (H+L) and goat anti-rabbit IgG (H+L) were obtained from Bio-Rad (Hercules, CA, USA). Fetal bovine serum was obtained from Atlanta Biologicals (Lawrenceville, GA, USA). Penicillin/streptomycin was from Corning (Manassas, VA, USA). Porous cubic Mn_2O_3 microparticles (1.5–2 μm) were synthesized as described previously [37]. Anti-cancer drug BA-TPQ was synthesized as described previously [47] (see Supplementary Material for details).

2.2 Fabrication of intracellular degradable hydrogel cubes

Biodegradable hydrogel cubes were prepared as reported previously [38]. Briefly, PEI was absorbed onto the porous surfaces of Mn_2O_3 inorganic templates from 1.5 mg mL-1 aqueous polymer solution for 1 h. The PEI-coated particles were then alternatingly exposed to PMAA and PVPON solutions (1.5 mg mL^{-1}, 0.01 M phosphate, pH=3.6) to form hydrogen-bonded $(PMAA/PVPON)_5$ multilayers inside the particle pores. The subscript 5 denotes the number of (PMAA/PVPON) bilayers within the multilayer coating. Each polymer deposition was performed for 45 min, which included sonication for 15 min (Branson Ultrasonic Bath), followed by shaking for 30 min (1500 rpm, Corning Vortex Mixer). To remove excess polymer, particles were centrifuged at 6000 rpm for 5 min using an Eppendorf MiniSpin centrifuge and rinsed two times with a 0.01 M buffer at pH = 3.6. After formation of the $(PMAA/PVPON)_5$ multilayer on Mn_2O_3 particle surfaces, the inorganic template was dissolved by exposing the coated particles to 1 M HCl for 24 h followed by six rinses with DI water at pH = 2. Next, some carboxyl groups of the PMAA layers within the $(PMAA/PVPON)_5$ polymeric replicas were chemically crosslinked by exposure to a carbodiimide solution (5 mg mL^{-1}, pH = 5, 0.01 M phosphate) for 45 min followed by cystamine hydrochloride solution (1 mg mL^{-1}, pH = 5.8, 0.01 M phosphate) for 20 h. After cross-linking, polymeric particles were exposed to pH = 8 (0.01 M phosphate buffer) for 24 h to release PVPON from the crosslinked PMAA hydrogel cubes. The PMAA hydrogel cubes were incubated with 0.1 M EDTA solution at pH = 7 for three hours to remove residual manganese ions followed by dialysis in deionized (DI) water for 3 days using 1 mL Float-A-Lyzer tubes with MWCO = 20000 Da (Spectrum Labs). The PMAA hydrogel cubes were loaded with BA-TPQ drug by soaking the hydrogels in 0.2 mg mL^{-1} BA-TPQ/methanol solution for 48 h in the dark followed by rinsing with pH = 7.4 (0.01 M phosphate) to remove excess BA-TPQ. The amount of encapsulated BA-TPQ was determined with UV-vis spectroscopy at 350 nm. BA-TPQ loading capacity was calculated as the ratio of $[(BA\text{-}TPQ)_i\text{-}(BA\text{-}TPQ)_s]$/[number of particles], where $(BA\text{-}TPQ)_i$ and $(BA\text{-}TPQ)_s$ are the initial BA-TPQ concentration and the BA-TPQ concentration in supernatant after BA-TPQ-loaded cubes were separated from solution, respectively.

2.3 Scanning electron microcopy (SEM)

Morphology and shape of PMAA microgels and BA-TPQ-microgel cubes were investigated with FEI Quanta™ FEG SEM microscope at 10 kV. For solution samples, a drop of hydrogel suspension was deposited on a silicon wafer and dried overnight at room temperature, while for freeze-dried samples, particle powder was dropped onto a piece of silicon wafer. Specimens were sputter-coated with an approximately 5 nm thick silver layer using a Denton sputter-coater before imaging.

2.4 Turbidimetry

Glutathione-triggered microgel degradation was examined with fluorometry (Varian, Cary Eclipse) by monitoring the turbidity change at 37 °C. The scattering intensity of microgel suspension (1.2×10^8 hydrogels/mL) at pH = 7.4 in PBS with or without 5 mM glutathione was measured at $\lambda = 700$ nm. The ratio of the hydrogel scattering intensity at a certain time point to that of the initial non-degraded hydrogel was used to calculate the relative turbidity.

2.5 ζ-Potential measurements

ζ-potential of microgel before and after BA-TPQ encapsulation was determined using a Nano Zetasizer (Malvern). The empty and BA-TPQ-loaded microgels were suspended in pH = 7.4 phosphate buffer solution, respectively, and their ζ-potential value was obtained by averaging three independent measurements.

2.6 *In-vitro* drug release

The BA-TPQ release studies were performed by the typical dialysis method [48,49]. 1.5 mL of BA-TPQ-microgel suspension ($(3\sim4)\times10^8$ hydrogels/mL) was placed in a dialysis bag (MWCO: 25 000 Da) and dialyzed against 40 mL of 0.01 M phosphate buffers in a shaking (50 rpm) water bath to ensure sink condition in which the solution pH was 7.4 (20 °C and 37 °C), 5 (37 °C) and 2 (37 °C), respectively. To study the redox-triggered BA-TPQ release, the releasing medium was prepared by adding 5 mM of GSH into 0.01 M phosphate buffer followed by adjusting pH to 7.4 (37 °C). At predetermined time intervals, 3 mL of external solution was taken and measured by UV-vis spectroscopy (Varian Cary 50).

2.7 Cell studies

2.7.1 Cell culture—Human normal hepatocyte cell lines (LO2 and CL48), human hepatocellular carcinoma cell lines (HepG2 and Huh7) and human intestinal epithelial cell line Caco-2 were obtained from American Type Culture Collection (Rockville, MD, USA). The LO2, CL48, HepG2 and Huh7 cells were cultured in Dulbecco's modified Eagle's media (DMEM). Caco-2 cells were grown in Eagle's minimum essential medium (EMEM). All cell culture media were supplemented with 10% fetal bovine serum and 1% penicillin/streptomycin.

2.7.2 Caco-2 cell monolayer permeability assay—The Caco-2 cell monolayer permeability assay was performed as described previously [50]. In brief, Caco-2 cells (4×10^5/well) were seeded on polycarbonate 6-well Transwell® inserts (Corning Costar Inc., NY, USA) and formed a confluent monolayer over 12 days prior to the permeability studies.

The transepithelial electrical resistance (TEER) of the monolayer, which indicates the formation of the monolayer and its integrity, was monitored using an epithelial voltohmmter (EVOM, WPI Inc., USA). The experiments were performed in HBSS supplemented with 30 mM HEPES at pH 6.0. Both BA-TPQ (5 μg/mL) and BA-TPQ-microgel cubes (with equivalent BA-TPQ concentration, 5 μg/mL) were added to the apical side of the membrane, and the transport of the compound from the apical compartment to the basolateral compartment was monitored over a 120 min time period using an HPLC method [8,44]. The apparent permeability coefficient (P_{app}) was calculated using the following equation: $P_{app} = (\partial Q/\partial t)/(A \times C_0)$, where '$\partial Q/\partial t$' is the permeability rate of the compound across the cells, 'A' is the diffusion area of the cell monolayer, and 'C_0' is the initial concentration of the compound in the apical compartment.

2.7.3 Viability assessment—The viability of BA-TPQ and BA-TPQ-microgel cubes against human hepatocyte cell lines (LO2 and CL48) and hepatocellular carcinoma cell lines (HepG2 and Huh7) were investigated using the MTT assay. In brief, the cells were seeded in a 96-well plate ($3–4 \times 10^3$ cells/well) and treated with various concentrations (0, 0.01, 0.02, 0.05, 0.1, 0.2, 0.5, 1 and 2 μg/mL) of BA-TPQ and BA-TPQ-microgel cubes. After 72 h incubation, 10 μL of MTT solution (5 mg mL^{-1}, Sigma-Aldrich Co.) were added to each well. The plates were then incubated for 2–4 h at 37°C. The supernatant was carefully removed, and the formazan crystals were dissolved in 100 μL DMSO. Absorbance was determined at λ = 570 nm using a SYNERGY Mx microplate reader (BioTek, Winooski, VT, USA). The cell survival percentages were calculated by dividing the mean OD of the compound containing wells by that of hydrogel-treated control wells.

2.7.4 Western blot analysis—The cells ($3–4 \times 10^5$ cells/dish) were seeded into 6-cm dishes and treated with various concentrations (0, 0.1, and 0.5 μg/mL) of BA-TPQ and BA-TPQ-cubes for 24 h. The cells were lysed in NP40 lysis buffer containing a protease inhibitor mixture (Sigma, St. Louis, MO, USA). Cell lysates were fractionated with identical amounts of protein by SDS-PAGE and transferred to Bio-Rad trans-Blot nitrocellulose membranes (Bio-Rad Laboratories, Hercules, CA) as described previously [51,52]. The nitrocellulose membrane was then incubated in blocking buffer (Tris-buffered saline containing 0.1% Tween 20 and 5% nonfat milk) for 1 h at room temperature. Then the membrane was incubated with the appropriate primary antibody overnight at 4°C with gentle shaking. The membrane was washed three times with rinsing buffer (Tris-buffered saline containing 0.1% Tween 20) for 15 min, and then was incubated with goat anti-mouse/rabbit IgG-horseradish peroxidase-conjugated antibody (Bio-Rad, Hercules, CA) for 1 h at room temperature. After repeating the washes in triplicate, the protein of interest was detected using enhanced chemiluminescence reagents from PerkinElmer LAS, Inc (Boston, MA). The intensity ratio under each band was determined by IMAGEJ software analysis normalized to untreated control.

2.8 Statistical analysis

The data were analyzed using the Prism software program version 6 (Graph Pad software Inc., San Diego, CA, USA). The Student's two-tailed *t*-tests were used for comparisons

between two groups. All quantitative data are expressed as the means ± SD from at least three independent experiments. $P < 0.05$ was considered to be statistically significant.

3. Results and Discussion

3.1 Fabrication of BA-TPQ-hydrogel cubes

Cubical PMAA microgel cubes were prepared by using a template-assisted LbL technique (Scheme 1) as developed in our previous studies [37,38]. The BA-TPQ was encapsulated into the PMAA microgel cubes via post-loading in methanol due to the poor solubility of BA-TPQ (even in the salt form) in water. Figures 1a and 1b demonstrate that the BA-TPQ-hydrogels became brownish after the drug loading compared to their initial white color which indicated a successful encapsulation of BA-TPQ. The hydrogel drug loading capacity was determined to be $(2.92 \pm 0.98) \times 10^{-4}$ ng BA-TPQ per particle, which is 2.3-fold smaller than that of doxorubicin (DOX; $(6.8 \pm 0.2) \times 10^{-4}$ ng DOX per particle) reported in our previous work [38]. This difference in loading between BA-TPQ and DOX can be attributed to a different loading pathway for hydrophobic and hydrophilic compounds into the PMAA hydrogel network. The cationic hydrophilic DOX can ionically bind to negatively charged PMAA groups in the hydrogel at physiological pH, while the BA-TPQ association in the porous PMAA network occurs mostly due to hydrophobic interactions between the drug and the hydrophobic segments of the PMAA network including methyl groups and -$(CH_2)_2$-S-S-$(CH_2)_2$- cystamine links. Figure 1c shows that the PMAA cubes before and after BA-TPQ loading have a similar size at pH = 7.4 (3.5 ± 0.2 and 3.5 ± 0.2 μm, respectively), at pH = 5 (2.2 ± 0.2 and 2.2 ± 0.2 μm, respectively), and at pH = 2 (2.5 ± 0.2 and 2.4 ± 0.2 μm, respectively) indicating the negligible electrostatic interactions between BA-TPQ and PMAA networks.

The 1.6-fold increase in the BA-TPQ-hydrogel cube size when pH is increased from pH = 5 to pH = 7.4 is attributed to swelling of the hydrogel due to ionization of the PMAA. In addition, the drug-loaded hydrogel swells 1.1-fold when the solution pH is decreased from 5 to 2 due to the protonation of primary amine groups from singly attached cystamine in the hydrogel network. Despite that, the BA-TPQ-loaded cubes retained their cubic shape upon the cubes swelling at pH = 7.4 and pH = 2, and a slight 12%-shrinkage at pH = 5, indicating that the physical entrapment of BA-TPQ does not affect the particle shape in solution. A similar surface charge of PMAA cubes before and after BA-TPQ loading of −23 ± 1 and −22 ± 2 mV, respectively, obtained via ζ-potential measurements of the particles at pH = 7.4 also points to mainly hydrophobic interactions between the drug and the PMAA network (Fig. S2). Despite the lower loading capacity for hydrophobic BA-TPQ, the PMAA hydrogel cubes still demonstrate the capability to load both hydrophilic and hydrophobic therapeutics ensuring their versatility for drug encapsulation. It is important to note that unlike micelles and polymersomes/liposomes in which the hydrophobic drug is encapsulated within the limited space of the hydrophobic cores (micelles) or membrane shell (polymersome/liposomes) [53], the PMAA hydrogel cubes are porous and uniform throughout the network, leading to a homogeneous encapsulation of hydrophobic molecules through the particle volume. The fluorescent image (Fig. S3) of hydrophobic Nile Red loaded hydrogel further proves that a hydrophobic agent can uniformly distribute in the hydrogel network since the

red fluorescence is observed throughout the hydrogel. Thus, the PMAA hydrogel cubes can achieve improved hydrophobic drug encapsulation compared to other popular systems.

Additionally advantageous is the ability of BA-TPQ-hydrogel cubes to preserve their negative surface charge since it is considered to be more preferable for clinical applications. It has been shown that positive charges may lead to severe immune responses and short blood circulation times [54]. Moreover, anionic drug delivery vehicles have been shown to accumulate preferentially in liver tissue [55] which is desirable for a liver cancer treatment through various administration methods including intravenous injection and oral administration [56,57].

The interaction of BA-TPQ with the PMAA hydrogel cubes manifested itself as a change in ensemble behavior of the particles as seen in SEM images of the particles air-dried from solutions on the surfaces of Si wafers (Fig. 2). Although the PMAA hydrogels maintained their 3-dimensional (3D) cubic structure (Fig. 2a and b) upon drying, the cubes appeared connected to each other, indicating capillary motion of water through the narrow pores of the matrix between the closely sitting PMAA hydrophilic particles during drying. In contrast, BA-TPQ-hydrogel cubes exhibited clearly defined particle edges (Fig. 2c and d) due to a more hydrophobic network obtained after encapsulation of BA-TPQ in the hydrogel. A similar observation has been made for gel composites where the inclusion of inorganic nanoparticles decreased the fusion of polymer microgels [58,59].

These results are also consistent with previous studies where the loading of small hydrophobic molecules or large proteins into a multilayer capsule shell increased the capsule rigidity [60–62]. In the case of the PMAA cubes, the interconnected multilayer hydrogel network provides an increased surface area for interaction with BA-TPQ and therefore the encapsulated BA-TPQ provides reinforcement to the hydrogel network throughout the entire particle volume.

Remarkably, the drying-induced association of the PMAA hydrogel cubes is reversible and the freeze-dried hydrogels can be easily re-dispersed as individual cubes in solution. This can be seen in SEM analysis of the freeze-dried PMAA hydrogel and BA-TPQ-hydrogel cubes (Fig. 3) which revealed particle clusters upon their lyophilization. Even though the edges and vertices of the cubes can be still observed (Fig. 3a), the PMAA hydrogels are seemingly deformed due to dehydration during freeze-drying. In contrast, the BA-TPQ-hydrogels exhibited well-preserved cubical geometry (Fig. 3d) with no deformations or morphology changes after freeze-drying. After rehydration in solutions at pH = 7.4 followed by air-drying on Si wafers, both PMAA hydrogel and BA-TPQ-hydrogel particles regained their cubical shape (Fig. 3b and 3e, respectively). Optical microscopy of the particles re-suspended in solution revealed that they can be easily re-dispersed without any aggregation with an average size of 3.5 ± 0.2 μm (Fig. 3c and f). In addition, the dramatic 17.3-fold increase in particle volume from $V_d = 2.46\ \mu m^3$ in the dry state, where $V = a^3$ and a is the average size of the cube's edge ($a = 1.35$ μm in dry state) to $V = 42.51\ \mu m^3$ in the hydrated state at pH = 7.4 was observed due to the hydrophilicity and deprotonation of the porous PMAA network at pH = 7.4 indicating their ability to absorb water even after being impregnated with the hydrophobic drug. This property is favorable for *in-vivo* drug delivery

since the hydrophilic carriers have demonstrated improved biocompatibility and can reduce non-specific protein adsorption [63,64]. These results demonstrate the structural robustness and versatility of the hydrogel cubes which can be dried for storage and later re-dispersed into solution without adverse effects on the particle size, shape, and morphology.

In addition, among vascular carriers designed by nature, red blood cells have an average diameter of ~7 μm and thickness of ~2 μm and function as natural carriers of oxygen in blood stream. Their elasticity allows their navigation through the vascular channels of varied sizes. Therefore, the inherent elasticity of the polymeric hydrogels over rigid particles is among their main advantages as the micrometer-size hydrogels have been demonstrated to squeeze through the channels of smaller sizes and restore their shape upon their entry from narrow to wider capillaries [65,66]. Therefore, we believe that the hydrogel of 2 μm presented in this work can be applied via an intravenous injection. Importantly, the PMAA hydrogel particle size can be further decreased down to a sub-micron size (*e.g.*, 0.6 μm) which is suitable for *in vivo* studies. Since the BA-TPQ encapsulation within the hydrogel network is due to the physical adsorption that is determined by the porosity and composition of the hydrogel, the ability of PMAA hydrogel for BA-TPQ encapsulation should not be significantly affected by the smaller particle size.

3.2 Redox-triggered degradation of BA-TPQ-hydrogels and drug release

The difference in redox potentials between intra- and extracellular environments is often utilized for controlled drug release to improve the efficacy of anticancer drug delivery [25,67]. To evaluate the degradation of the PMAA hydrogel and BA-TPQ-hydrogel cubes, the relative turbidity of their suspensions was determined under intracellular conditions as the ratio of scattering intensity of the sample solution at various time points to that of the initial sample solution. In the absence of reducing agent GSH, the relative solution turbidity of PMAA hydrogels used as controls did not change during the entire experiment indicating the stability of the hydrogel without the redox-trigger (Fig 4a, squares). In contrast, empty and drug-loaded hydrogels were completely degraded after 3 hour-exposure to the intracellular-mimicking environment (5 mM GSH, 0.01 M phosphate buffer, pH = 7.4) (Fig. 4a, circles and triangles, respectively). The plain PMAA hydrogels degraded faster than BA-TPQ-hydrogel cubes showing only 20 ± 2% relative turbidity after 40 min GSH treatment versus 55 ± 1% in the case of BA-TPQ-hydrogels. The delayed degradation of BA-TPQ-hydrogel cubes can be explained by the limited GSH diffusion into the network after BA-TPQ encapsulation due to the increased hydrophobicity discussed above. Since typical GSH concentration in cytoplasm (~2–10 mM) is 1000 times higher than that in the extracellular environment (~ 2–20 μM), and tumor cells exhibit GSH concentrations 4 times higher than normal cells [68], the BA-TPQ-hydrogels can be used for controlled drug release inside cancer cells. Also, since the degradation of the BA-TPQ-hydrogel cubes results in release of PMAA chains with low molecular weight (20,000 Da), they can be easily eliminated by renal clearance preventing side-effects to normal tissues [69].

The BA-TPQ release from the hydrogel cubes was studied using UV-Vis spectroscopy. Figure 4b shows that less than 3% BA-TPQ had been released to the medium (PBS, pH = 7.4) after their incubation at 20 °C 24 h (Fig. 4b, squares) demonstrating the potential for in-

solution storage of the drug-loaded hydrogel cubes. Moreover, at physiological temperature (37 °C), the BA-TPQ release was only 9.5 ± 0.6 % at pH = 7.4 (circles), 8.8 ± 2% at pH = 5 (up-triangles) and 10 ± 2% at pH = 2 (down-triangles) after 24-h incubation (Fig. 4b). The slight increase of BA-TPQ release at 37 °C compared to that at 20 °C is attributed to a better solubility of the drug at the increased temperature. In contrast to the hydrophobic drug paclitaxel whose sustained release from mucin hydrogels reached 77 ± 5% after 7 days [70], the release of BA-TPQ in this work plateaued after three days and resulted in overall drug release of 14 ± 2% at pH = 7.4, 11 ± 3% at pH = 5, and 13 ± 3% at pH = 2. These results also demonstrate that the BA-TPQ release is independent of the environmental pH despite the pH-triggered size changes of the hydrogel cubes. This excellent BA-TPQ retention by the PMAA multilayer hydrogels ensures no premature drug leakage *in vivo* in response to pH variations. Conversely, significant acceleration of BA-TPQ release from the hydrogel cubes was observed in the presence of 5 mM GSH (Fig. 4b, diamonds) when 40 ± 9% and 77 ± 3% of the encapsulated BA-TPQ could be detected in the medium after 6 and 24 h of incubation at 37 °C, respectively. The delayed release of BA-TPQ over 24 hours compared to the BA-TPQ-hydrogel degradation observed over only 3 hours in turbidity measurements (Fig. 4a) can be explained by the additional time necessary for BA-TPQ diffusion across the dialysis membrane into the receiving media. The observed delay in the drug release would therefore not be expected in a real biological environment since the hydrogel degradation and subsequent release of BA-TPQ will occur in the cellular cytosol upon the cleavage of disulfide links in the intracellular reducing environment.

3.3 Enhanced permeability of encapsulated BA-TPQ through epithelial cell monolayers

The potential of the BA-TPQ-hydrogel cubes for oral delivery of the drug has been explored as a highly attractive route of drug administration due to convenience and patient compliance [21,71]. First, the BA-TPQ release profile demonstrated that the encapsulated drug is well shielded by the hydrogel matrix at pH = 2 with only 5.2 ± 0.6% of BA-TPQ release during 4 h (Fig. 4b). This result indicates excellent potential for BA-TPQ-hydrogel cubes as oral delivery agents of anticancer therapeutics since the retention time in the stomach ranges from 30 min to 4 h [72]. The permeability of BA-TPQ itself and that delivered by the PMAA hydrogel cubes was investigated across Caco-2 cell monolayers, as the Caco-2 model has been widely applied for the evaluation of permeability and absorption capacity of orally administered drugs [73]. To determine the integrity of the Caco-2 cell monolayer during the sample permeability experiments, the trans-epithelial electrical resistance (TEER) of the cell monolayer was measured. Remarkably, no significant changes in TEER were found in any treatment groups, which implies that both pristine BA-TPQ and BA-TPQ-hydrogel cubes did not reduce the monolayer integrity or induce opening of the tight intercellular junctions during the drug transport. Moreover, the encapsulation of BA-TPQ into PMAA hydrogel cubes significantly increases the trans-epithelial transport of the drug in a time-dependent manner (Fig. 5). The apparent permeability coefficient (P_{app}) of BA-TPQ-encapsulated in the hydrogel cubes was measured to be 2.82×10^{-6} cm/s after 2 hours of incubation of the BA-TPQ-hydrogel sample with the cells which is 1.8-fold higher than that for pristine BA-TPQ at $P_{app} = 1.59 \times 10^{-6}$ cm/s ($P < 0.01$). This result indicates the enhanced permeability of BA-TPQ through the cell monolayer mediated by the PMAA hydrogel matrix. The improved transmembrane transport of encapsulated therapeutic agents

in contrast to unshielded drugs was reported previously, and was attributed either to the absorption/bio-adhesion enhancements or to an incremental internalization of drug carriers [74]. In this case, the use of the PMAA matrix may favor the transmembrane permeability as PMAA is a bio-adhesive material which can facilitate the adhesion to mucus layers [75] and therefore promote the *in vivo* absorption of loaded cargo.

3.4 Amplified toxicity of encapsulated BA-TPQ to liver cancer cells

To assess the anticancer properties of BA-TPQ-hydrogel cubes, we investigated the cytotoxicity of BA-TPQ-hydrogels to hepatocyte (LO2 and CL48) and hepatocellular carcinoma (HepG2 and Huh7) cell lines as they can produce an *in vitro* metabolic profile similar to that seen *in vivo* for a given drug [76]. The HepG2 and Huh7 cancer cell lines were selected based on their different genetic background with the former and the latter of p53 wild-type and p53 mutant status, respectively.

BA-TPQ exhibited a dose-dependent cytotoxicity to the experimental cell lines where an increase in BA-TPQ loading concentration resulted in reduced cell viability (Fig. 6). Importantly, the half-maximal inhibitory concentration (IC_{50}) values of BA-TPQ for LO2 (1.95 ± 0.24 μg/mL) and CL48 (1.71 ± 0.26 μg/mL) hepatocytes (normal liver cells) were 2.3-fold ($P < 0.05$) and 2.1-fold ($P < 0.05$) higher than that for HepG2 carcinoma cells (IC_{50} = 0.83 ± 0.08 μg/mL) indicating the selectivity of BA-TPQ to liver cancer cells. The BA-TPQ selectivity was also observed for another liver cancer cell line, p53-mutant Huh7, where the IC_{50} value of 0.46 ± 0.04 μg/mL was 4.2- fold ($P < 0.01$) and 3.7-fold ($P < 0.01$) lower than the IC_{50} values of BA-TPQ for LO2 and CL48 normal liver cells, respectively (Fig. 6). These results agree with the previous reports on the selective toxicity of BA-TPQ against breast cancer cells MCF-7, MCF-7 p53 KD and MDA-MB-468 in contrast to non-malignant breast epithelial cells MCF-10A [8].

Importantly, the encapsulated BA-TPQ did not cause elevated cytotoxicity in CL48 and LO2 hepatocyte (normal liver cell) cultures and demonstrated similar cell viability profiles to non-encapsulated drug with the corresponding IC_{50} values of 1.46 ± 0.12 and 1.57 ± 0.11 μg/mL, respectively, while IC_{50} values of 1.71 ± 0.26 and 1.95 ± 0.24 μg/mL, respectively, were obtained for non-encapsulated BA-TPQ (Fig. 6a and b). In contrast, BA-TPQ-hydrogel cubes were significantly ($P < 0.05$) more potent in decreasing the viability of HepG2 and Huh7 liver cancer cells compared to non-encapsulated BA-TPQ. For example, the IC_{50} values for BA-TPQ-hydrogels were 0.52 ± 0.03 μg/mL in the case of HepG2 and 0.29 ± 0.01 μg/mL in the case of Huh7, while these values were almost 40% higher when non-encapsulated BA-TPQ was used resulting in the IC_{50} of 0.83 ± 0.08 and 0.46 ± 0.04 μg/mL for HepG2 and Huh7, respectively (Fig. 6, $P < 0.05$). These results agree with the previously reported enhanced therapeutic effect for encapsulated drugs explained by the improved bioavailability of hydrophobic drugs through solubilizing by and non-specific cellular internalization of drug carriers [77,78]. Similarly, in this work, the enhanced BA-TPQ anticancer activity is due to the relatively high hydrophilicity of BA-TPQ-hydrogels unlike BA-TPQ and due to the carrier-assisted transportation of hydrophobic drug across the cell membrane. In addition, the cubical shape of the carrier can be important in promoting the cellular uptake of the carrier leading to the augmented transport of BA-TPQ. The larger

contact area of rod- and disc-shaped particles has been shown to improve particle adhesion to a cell membrane, and subsequently, to enhance cellular internalization of the particles [79]. Computational simulations by Gompper *et al* also predicted favorable membrane attachment of a cubical particle due to the higher adhesion strength compared to that of a spherical particle [80]. In this work, the flat faces of the PMAA hydrogel cubes can provide a large surface area for cell interactions and also facilitate BA-TPQ transmembrane transport at the particle-cell interfaces. In addition, the redox-induced degradation of BA-TPQ-hydrogels enables rapid drug release inside the cells which improves the anti-tumor effectiveness of the drug. It is noteworthy that BA-TPQ-hydrogel cubes display excellent inhibitory effects in both p53 wide-type (HepG2) and p53-mutant (Huh7) liver cancer cells indicating a p53-independent antitumor activity. Since the p53 mutation commonly occurs in HCC which may promote tumorigenesis and is associated with poor therapeutic outcomes [81], BA-TPQ-hydrogel cubes can be a successful candidate for HCC treatment due to their p53-independent antitumor activity.

The enhanced cytotoxicity of BA-TPQ against cancer cells can be attributed to suppression of MDM2 protein expression amplified in tumor cells. Similarly, the recently discovered SP141 and JapA MDM2 inhibitors were reported to have increased toxicities to pancreatic and breast cancer cells [68,71] demonstrating that the tumor selectivity in cancer therapy can be achieved by targeting MDM2 protein expression. Our results show that the tumor toxicity of BA-TPQ is amplified after the encapsulation of the drug into PMAA hydrogel cubes with minimal adverse effects on the growth of normal liver cells.

3.5 Regulation of tumor protein expression by BA-TPQ-hydrogel cubes

MDM2 protein overexpression is known to be associated with invasive tumors, high grade/late stage tumors, cancer recurrence, and metastasis in HCC patients, which makes it a promising target for HCC treatment [50]. Since BA-TPQ inhibits tumor growth via multiple pathways including the down-regulation of MDM2 [51,52], the ability of BA-TPQ-hydrogels to regulate expression of MDM2 and related proteins was evaluated. As shown in Figure 7, BA-TPQ-hydrogels significantly inhibited the MDM2 expression and activated wild-type p53 and p21 expression at 0.1 μg/mL ($P < 0.05$), while free BA-TPQ did not show or showed slight effects at the same concentration. In HepG2 cells, after the exposure to BA-TPQ-hydrogel cubes at 0.1 and 0.5 μg/mL concentrations, the MDM2 protein level was decreased by 57% ($P < 0.01$) and 94% ($P < 0.01$), respectively (Fig. 7b). At the same time, the expression of p53 which is known as a tumor suppressor and p21 which prevents cell proliferation were increased by 2.5- (p53) ($P < 0.01$) and 2-fold (p21) ($P < 0.01$) at 0.1 μg/mL of BA-TPQ-hydrogel treatment, and by 3.9- (p53) ($P < 0.01$) and 3.2-fold (p21) ($P < 0.01$) at 0.5 μg/mL of BA-TPQ-hydrogel treatment (Fig. 7c and d), respectively.

The effect of encapsulation on the ability of BA-TPQ to down-regulate MDM2 and upregulate the expression of p53 and p21 in HepG2 cells is highly pronounced. In the tests, pristine non-encapsulated BA-TPQ demonstrated lower levels of down-regulation of MDM2 expression with only 28% (0.1 μg/mL BA-TPQ) ($P < 0.05$) and 69% (0.5 μg/mL BA-TPQ) ($P < 0.01$), respectively (Fig. 7b). Similar trends were found in the upregulation of p53 and p21 expression. Treatment with the non-encapsulated BA-TPQ resulted in 1.9- ($P < 0.01$)

and 2.3-fold ($P < 0.01$) increased levels of p53 (Fig. 7c) and in 1.4- and 2.3-fold ($P < 0.05$) increase in p21 levels at 0.1 and 0.5μg/mL BA-TPQ, respectively (Fig. 7d).

In p53-mutant Huh7 cells, BA-TPQ-hydrogels also demonstrated superior inhibition of MDM2 and promotion of p21 expression in contrast to non-encapsulated BA-TPQ. The levels of MDM2 decreased by 46 and 77% after treatment with 0.1 and 0.5 μg/mL BA-TPQ-hydrogels ($P < 0.01$), respectively, while only 29% ($P < 0.05$) and 53% ($P < 0.01$) of MDM2 downregulation was observed for BA-TPQ at 0.1 and 0.5 μg/mL, respectively (Fig. 7e). The increase by 1.7- ($P < 0.05$) and 2.8-fold ($P < 0.01$) in the p21 levels was achieved using BA-TPQ-hydrogels at 0.1 and 0.5 μg/mL, respectively, with only 1- and 1.9-fold ($P < 0.05$) upregulation in p21 at the corresponding concentrations of BA-TPQ (Fig. 7g).

Interestingly, no effect of BA-TPQ on p53 expression was observed in Huh7 cells (Fig. 7f) even when MDM2 expression was suppressed (Fig. 7e). As reported previously [82], mutant p53 proteins can both lose their tumor suppressive functions and become oncogenic. The results demonstrate that BA-TPQ can suppress MDM2 expression regardless of p53 status. This agrees with previous reports where MDM2 was shown to exhibit both p53-dependent and independent activities to facilitate tumor growth and metastasis [51–83]. The inhibition of MDM2 can increase p53 expression, leading to the apoptosis of cancer cells [83]. Also, recent studies have demonstrated that novel MDM2 inhibitors are able to bypass the MDM2-p53 pathway to exert antitumor activity [51,52].

The protein expression analysis verifies the greatly enhanced inhibition activity of BA-TPQ-hydrogel cubes on MDM2 protein expression and indicates that this inhibition is independent of p53 status. That along with lower IC_{50} values found for BA-TPQ hydrogels incubated with HepG2 and Huh7 liver cancer cells indicates superior antitumor efficacy of the BA-TPQ- hydrogel cubes compared to non-encapsulated BA-TPQ. These results demonstrate that using the PMAA hydrogel cubes as a drug carrier can greatly improve the ability of BA-TPQ to regulate oncoprotein expression in liver cancer cells and that BA-TPQ hydrogel cubes are a highly promising tool for clinical liver cancer therapy due to their remarkable anticancer effectiveness.

4. Conclusions

A novel delivery platform has been demonstrated for a highly potent anticancer drug, BA-TPQ, using PMAA hydrogel particles of micrometer size and cubical shape as the drug encapsulating matrix. The cubical porous hydrogel particles were obtained via template-assisted multilayer assembly of hydrogen-bonded PMAA with PVPON into porous network of sacrificial manganese oxide particles followed by chemical crosslinking of PMAA chains with cystamine, release of PVPON from the PMAA network and dissolution of the inorganic template. The obtained multilayer PMAA hydrogels of cubical shape can be effectively loaded with BA-TPQ without changing their shape and pH-regulated size. The BA-TPQ-hydrogels demonstrated enhanced structural rigidity and could maintain their 3D shape and morphology after air-drying, lyophilization, and resuspension in solution which can be crucial for prolonged shelf-storage. Conversely, rapid degradation of BA-TPQ-hydrogel cubes occurs in the presence of intracellular concentrations (5 mM) of the reducing agent

glutathione with approximately 80% BA-TPQ release within 24 h of *in vitro* incubation. The encapsulation of BA-TPQ into PMAA hydrogel cubes was also found to significantly increase the trans-epithelial transport of the drug via monolayers of Caco-2 cells used as a model for the evaluation of permeability and absorption capacity of orally administered drugs. The apparent permeability coefficient of BA-TPQ-microgel cubes was found to be 2.82×10^{-6} cm/s which was ~2-fold higher than that of non-encapsulated BA-TPQ. Finally, BA-TPQ-hydrogel cubes improve the cellular uptake of BA-TPQ. BA-TPQ-hydrogel cubes exhibit superior anticancer effect against HepG2 (IC_{50} = 0.52 μg/mL) and Huh7 (IC_{50} = 0.29 μg/mL) hepatocellular carcinoma cells with a 40% decrease in the IC_{50} values compared to those of non-encapsulated BA-TPQ. Non-malignant liver cells, LO2 and CL48, have lower sensitivity to BA-TPQ-hydrogel cubes with the IC_{50} values being twice those of hepatoma cells which indicates a good selectivity of BA-TPQ-hydrogel cubes to the cancer cells. In addition, the encapsulation of BA-TPQ within a porous network of PMAA hydrogel cubes significantly amplifies the potency of BA-TPQ to down-regulate MDM2 oncogenic protein and upregulate the expression of p53 (a tumor suppressor) and p21 (cell proliferation suppressor) in HepG2 cells. Of special note, the enhanced inhibition of MDM2 protein expression by BA-TPQ-hydrogel cubes was found to be independent of p53 status in Huh7 liver cancer cells. We believe that our novel drug delivery platform for the highly potent anticancer drug BA-TPQ provides a facile method for encapsulation of hydrophobic drugs and can facilitate enhanced efficacy for liver cancer therapy. The integration of redox-sensitivity of the hierarchically assembled multilayer hydrogel matrix with controlled non-spherical shape may allow combining well-regulated drug release with shape-modulated drug delivery for clinical liver cancer treatment.

Supplementary Material

Refer to Web version on PubMed Central for supplementary material.

Acknowledgments

This work was supported by NSF Career Award #1350370 (EK) and by a Collaborative Programmatic Development grant from the UAB Comprehensive Cancer Center (SV), and by Award #1UL1RR025777 from the NIH National Center for Research Resources (SV). This work was also supported by the National Institutes of Health (NIH) grant R01 CA186662 (RZ). The content is solely the responsibility of the authors, and do not necessarily represent the official views of the National Institutes of Health. This work was also supported by American Cancer Society (ACS) grant RSG-15-009-01-CDD (WW). We thank Mr. Fei Liu (UAB), Mr. Aaron Alford (UAB) and Mr. Theron Anderson (UAB) for technical assistance. The UAB SEM and High Resolution Imaging facility is also acknowledged.

References

1. Mittal S, El-Serag HB. Epidemiology of HCC: consider the population. J Clin Gastroenterol. 2013; 47:S2. [PubMed: 23632345]
2. Zhu AX, Rosmorduc O, Evans TJ, Ross PJ, Santoro A, Carrilho FJ, Bruix J, Qin S, Thuluvath PJ, Llovet JM, Leberre MA, Jensen M, Meinhardt G, Kang YK. SEARCH: a phase III, randomized, double-blind, placebo-controlled trial of sorafenib plus erlotinib in patients with advanced hepatocellular carcinoma. J Clin Oncol. 2015; 33:559–566. [PubMed: 25547503]
3. Peck-Radosavljevic M. Drug therapy for advanced-stage liver cancer. Liver cancer. 2014; 3:125–131. [PubMed: 24945003]

4. Wang J, Zheng T, Chen X, Song X, Meng X, Bhatta N, Pan S, Jiang H, Liu L. MDM2 antagonist can inhibit tumor growth in hepatocellular carcinoma with different types of p53 in vitro. J Gastroen Hepatol. 2011; 26:371–377.
5. Ezell SJ, Li H, Xu H, Zhang X, Gurpinar E, Zhang X, Rayburn ER, Sommers CI, Yang X, Velu SE, Wang W, Zhang R. Preclinical pharmacology of BA-TPQ, a novel synthetic iminoquinone anticancer agent. Mar Drugs. 2010; 8:2129–2141. [PubMed: 20714427]
6. Chen D, Wang W, Qin JJ, Wang MH, Murugesan S, Nadkarni DH, Velu SE, Wang H, Zhang R. Identification of the ZAK-MKK4-JNK-TGFβ signaling pathway as a molecular target for novel synthetic iminoquinone anticancer compound BA-TPQ. Curr Cancer Drug Targets. 2013; 13:651–660. [PubMed: 23607596]
7. Wang W, Rayburn ER, Velu SE, Nadkarni DH, Murugesan S, Zhang R. In vitro and in vivo anticancer activity of novel synthetic makaluvamine analogues. Clin Cancer Res. 2009; 15:3511–3518. [PubMed: 19451594]
8. Wang W, Rayburn ER, Velu SE, Chen D, Nadkarni DH, Murugesan S, Chen D, Zhang R. A novel synthetic iminoquinone, BA-TPQ, as an anti-breast cancer agent: in vitro and in vivo activity and mechanisms of action. Breast Cancer Res Treat. 2010; 123:321–331. [PubMed: 19936915]
9. Wang F, Ezell SJ, Zhang Y, Wang W, Rayburn ER, Nadkarni DH, Murugesan S, Velu SE, Zhang R. FBA-TPQ, a novel marine-derived compound as experimental therapy for prostate cancer. Invest New Drugs. 2010; 28:234–241. [PubMed: 19274441]
10. Wang W, Qin JJ, Voruganti S, Wang MH, Sharma H, Patil S, Zhou J, Wang H, Mukhopadhyay D, Buolamwini J, Zhang R. Identification of a new class of MDM2 inhibitor that inhibits growth of orthotopic pancreatic tumors in mice. Gastroenterology. 2014; 147:893–902. [PubMed: 25016295]
11. Li H, Ezell SJ, Zhang X, Wang W, Xu H, Rayburn ER, Zhang X, Gurpinar E, Yang X, Sommers CI, Velu SE, Zhang R. Development and validation of an HPLC method for quantitation of BA-TPQ, a novel iminoquinone anticancer agent, and an initial pharmacokinetic study in mice. Biomed Chromatogr. 2011; 25:628–634. [PubMed: 20845374]
12. Hutchinson AD, Hosking JR, Kichenadasse G, Mattiske JK, Wilson C. Objective and subjective cognitive impairment following chemotherapy for cancer: a systematic review. Cancer Treat Rev. 2012; 38:926–934. [PubMed: 22658913]
13. Kanamala M, Wilson WR, Yang M, Palmer BD, Wu Z. Mechanisms and biomaterials in pH-responsive tumour targeted drug delivery: A review. Biomaterials. 2016; 85:152–67. [PubMed: 26871891]
14. Patel NR, Pattni BS, Abouzeid AH, Torchilin VP. Nanopreparations to overcome multidrug resistance in cancer. Adv Drug Deliv Rev. 2013; 65:1748–1762. [PubMed: 23973912]
15. Narasimhan B, Goodman JT, Vela Ramirez JE. Rational Design of Targeted Next-Generation Carriers for Drug and Vaccine Delivery. Annu Rev Biomed Eng. 2016; 18:25–49. [PubMed: 26789697]
16. Li W, Liu Q, Zhang P, Liu L. Zwitterionic nanogels crosslinked by fluorescent carbon dots for targeted drug delivery and simultaneous bioimaging. Acta Biomater. 2016; 40:254–262. [PubMed: 27063492]
17. Yan Y, Wang Y, Heath JK, Nice EC, Caruso F. Cellular association and cargo release of redox-responsive polymer capsules mediated by exofacial thiols. Adv Mater. 2011; 23:3916–3921. [PubMed: 21809395]
18. Liang X, Liu F, Kozlovskaya V, Palchak Z, Kharlampieva E. Thermoresponsive Micelles from Double LCST-Poly(3-methyl-N-vinylcaprolactam) Block Copolymers for Cancer Therapy. ACS Macro Lett. 2015; 4:308–311.
19. Liu F, Kozlovskaya V, Medipelli S, Xue B, Ahmad F, Saeed M, Kharlampieva E. Temperature-Sensitive Polymersomes for Controlled Delivery of Anticancer Drugs. Chem Mater. 2015; 27:7945–7956.
20. Gu D, O'Connor AJ, Qiao GGH, Ladewig K. Hydrogels with smart systems for delivery of hydrophobic drugs. Expert Opin Drug Deliv. 2016; 23:1–17.
21. Koetting MC, Peters JT, Steichen SD, Peppas NA. Stimulus-responsive hydrogels: Theory, modern advances, and applications. Mater Sci Eng R Rep. 2015; 93:1–49. [PubMed: 27134415]

22. Liu P, Luo Q, Guan Y, Zhang Y. Drug release kinetics from monolayer films of glucose-sensitive microgel. Polymer. 2010; 51:2668–2675.
23. Sun S, Wu P. A one-step strategy for thermal-and pH-responsive graphene oxide interpenetrating polymer hydrogel networks. J Mater Chem. 2011; 21:4095–4097.
24. Guan Y, Zhang Y. Boronic acid-containing hydrogels: synthesis and their applications. Chem Soc Rev. 2013; 42:8106–8121. [PubMed: 23860617]
25. Zhang X, Malhotra S, Molina M, Haag R. Micro-and nanogels with labile crosslinks–from synthesis to biomedical applications. Chem Soc Rev. 2015; 44:1948–1973. [PubMed: 25620415]
26. Saxena S, Hansen CE, Lyon LA. Microgel Mechanics in Biomaterial Design. Acc Chem Res. 2014; 47:2426–2434. [PubMed: 24873478]
27. Longmire MR, Ogawa M, Choyke PL, Kobayashi H. Biologically Optimized Nanosized Molecules and Particles: More than Just Size. Bioconjugate Chem. 2011; 22:993–1000.
28. Annabi N, Tamayol A, Uquillas JA, Akbari M, Bertassoni LE, Cha C, Camci-Unal G, Dokneci MR, Peppas NA, Khademhosseini A. 25th anniversary article: rational design and applications of hydrogels in regenerative medicine. Adv Mater. 2014; 26:85–124. [PubMed: 24741694]
29. Tumarkin E, Kumacheva E. Microfluidic generation of microgels from synthetic and natural polymers. Chem Soc Rev. 2009; 38:2161–2168. [PubMed: 19623340]
30. Sharpe LA, Daily AM, Horava SD, Peppas NA. Therapeutic applications of hydrogels in oral drug delivery. Expert Opin Drug Deliv. 2014; 11:901–915. [PubMed: 24848309]
31. Matsusaki M, Akashi M. Functional Multilayered Capsules for Targeting and Local Drug Delivery. Expert Opin Drug Deliv. 2009; 6:1207–1217. [PubMed: 19831583]
32. Del Mercato LL, Rivera-Gil P, Abbasi AZ, Ochs M, Gnas C, Zins I, Sönnichsen G, Parak WJ. LbL Multilayer Capsules: Recent Progress and Future Outlook for Their Use in Life Sciences. Nanoscale. 2010; 2:458–467. [PubMed: 20644746]
33. Delcea M, Möhwald H, Skirtach AG. Stimuli-responsive LbL Capsules and Nanoshells for Drug Delivery. Adv Drug Delivery Rev. 2011; 63:730–747.
34. Cui J, Richardson JJ, Björnmalm M, Faria M, Caruso F. Nanoengineered Templated Polymer Particles: Navigating the Biological Realm. Acc Chem Res. 2016; 49:1139–1148. [PubMed: 27203418]
35. Kharlampieva E, Kozlovskaya V, Sukhishvili SA. Layer-by-layer hydrogen-bonded polymer films: From fundamentals to applications. Adv Mater. 2009; 21:3053–3065.
36. Caruso F. Hollow Capsule Processing Through Colloidal Templating and Self-Assembly. Chem Eur J. 2000; 6:413–419. [PubMed: 10747405]
37. Kozlovskaya V, Chen J, Tedjo C, Liang X, Campos-Gomez J, Oh J, Saeed M, Lungu CT, Kharlampieva E. pH-Responsive Hydrogel Cubes for Release of Doxorubicin in Cancer Cells. J Mater Chem B. 2014; 2:2494–2507.
38. Xue B, Kozlovskaya V, Liu F, Chen J, Williams J, Campos-Gomez J, Saeed M, Kharlampieva E. Intracellular Degradable Hydrogel Cubes and Spheres for Anticancer Drug Delivery. ACS Appl Mater Interfaces. 2015; 7:13633–13644. [PubMed: 26028158]
39. Wang Y, Caruso F. Template Synthesis of Stimuli-Responsive Nanoporous Polymer-Based Spheres via Sequential Assembly. Chem Mater. 2006; 18:4089–4100.
40. Wang Y, Price AD, Caruso F. Nanoporous Colloids: Building Blocks for a New Generation of Structured Materials. J Mater Chem. 2009; 19:6451–6464.
41. Kozlovskaya V, Higgins W, Chen J, Kharlampieva E. Switching Shape of Layer-by-layer Hydrogel Microcontainers. Chem Commun. 2011; 47:8352–8354.
42. Kozlovskaya V, Wang Y, Higgins W, Chen J, Chen Y, Kharlampieva E. pH-Triggered Shape Response of Cubical Ultrathin Hydrogel Capsules. Soft Matter. 2012; 8:9828–9839.
43. Liang X, Kozlovskaya V, Chen Y, Zavgorodnya O, Kharlampieva E. Thermosensitive multilayer hydrogels of poly(N-vinylcaprolactam) as nanothin films and shaped capsules. Chem Mater. 2012; 24:3707–3719. [PubMed: 23087543]
44. Merkel TJ, Chen K, Jones SW, Pandya AA, Tian S, Napier ME, Zamboni WE, DeSimone JM. The effect of particle size on the biodistribution of low-modulus hydrogel PRINT particles. J Control Release. 2012; 162:37–44. [PubMed: 22705460]

45. Shimoni O, Yan Y, Wang Y, Caruso F. Shape-dependent cellular processing of polyelectrolyte capsules. ACS Nano. 2012; 7:522–530. [PubMed: 23234433]
46. Alexander JF, Kozlovskaya V, Chen J, Kuncewicz T, Kharlampieva E, Godin B. Cubical Shape Enhances the Interaction of Layer-by-Layer Polymeric Particles with Breast Cancer Cells. Adv Healthc Mater. 2015; 4:2657–2666. [PubMed: 26424126]
47. Shinkre BA, Raisch KP, Fan L, Velu SE. Analogs of the marine alkaloid makaluvamines: Synthesis, topoisomerase II inhibition, and anticancer activity. Bioorg Med Chem Lett. 2007; 10:2890–2893.
48. Li Z, Qiu L, Chen Q, Hao T, Qiao M, Zhao H, Zhang J, Hu H, Zhao X, Chen D, Mei L. pH-sensitive nanoparticles of poly(L-histidine)-poly(lactide-co-glycolide)-tocopheryl polyethylene glycol succinate for anti-tumor drug delivery. Acta Biomater. 2015; 11:137–150. [PubMed: 25242647]
49. Yang Q, Tan L, He C, Liu B, Xu Y, Zhu Z, Shao Z, Gong B, Shen YM. Redox-responsive micelles self-assembled from dynamic covalent block copolymers for intracellular drug delivery. Acta Biomater. 2015; 17:193–200. [PubMed: 25662913]
50. Voruganti S, Qin JJ, Sarkar S, Nag S, Walbi IA, Wang S, Zhao Y, Wang W, Zhang R. Oral nanodelivery of anticancer ginsenoside 25-OCH3-PPD, a natural inhibitor of the MDM2 oncogene: Nanoparticle preparation, characterization, in vitro and in vivo anti-prostate cancer activity, and mechanisms of action. Oncotarget. 2015; 6:21379–21394. [PubMed: 26041888]
51. Qin JJ, Wang W, Voruganti S, Wang H, Zhang WD, Zhang R. Identification of a new class of natural product MDM2 inhibitor: In vitro and in vivo anti-breast cancer activities and target validation. Oncotarget. 2015; 6:2623–2640. [PubMed: 25739118]
52. Qin JJ, Wang W, Voruganti S, Wang H, Zhang WD, Zhang R. Inhibiting NFAT1 for breast cancer therapy: New insights into the mechanism of action of MDM2 inhibitor JapA. Oncotarget. 2015; 6:33106–33119. [PubMed: 26461225]
53. Tang F, Li L, Chen D. Mesoporous silica nanoparticles: synthesis, biocompatibility and drug delivery. Adv Mater. 2012; 24:1504–1534. [PubMed: 22378538]
54. Wang AZ, Langer R, Farokhzad OC. Nanoparticle delivery of cancer drugs. Annu Rev Med. 2012; 63:185–198. [PubMed: 21888516]
55. Maeda H, Nakamura H, Fang J. The EPR effect for macromolecular drug delivery to solid tumors: Improvement of tumor uptake, lowering of systemic toxicity, and distinct tumor imaging in vivo. Adv Drug Deliv Rev. 2013; 65:71–79. [PubMed: 23088862]
56. Vinogradov SV. Colloidal microgels in drug delivery applications. Curr Pharm Des. 2006; 12:4703–4712. [PubMed: 17168773]
57. Caldorera-Moore M, Peppas NA. Micro-and nanotechnologies for intelligent and responsive biomaterial-based medical systems. Adv Drug Deliv Rev. 2009; 61:1391–1401. [PubMed: 19758574]
58. Xu J, Zeng F, Wu S, Liu X, Hou C, Tong Z. Gold nanoparticles bound on microgel particles and their application as an enzyme support. Nanotechnology. 2007; 18:265704. [PubMed: 21730408]
59. Agrawal M, Pich A, Gupta S, Zafeiropoulos NE, Rubio-Retama J, Simon F, Stamm M. Temperature sensitive hybrid microgels loaded with ZnO nanoparticles. J Mater Chem. 2008; 18:2581–2586.
60. Cui D, Jing J, Boudou T, Pignot-Paintrand I, De Koker S, De Geest BG, Picart C, Auzély-Velty R. Hydrophobic shell loading of biopolyelectrolyte capsules. Adv Mater. 2011; 23:H200–H204. [PubMed: 21590815]
61. Shen HJ, Shi H, Ma K, Xie M, Tang LL, Shen S, Li B, Wang XS, Jin Y. Polyelectrolyte capsules packaging BSA gels for pH-controlled drug loading and release and their antitumor activity. Acta Biomater. 2013; 9:6123–6133. [PubMed: 23271041]
62. Kurapati R, Raichur AM. Graphene oxide based multilayer capsules with unique permeability properties: facile encapsulation of multiple drugs. Chem Comm. 2012; 48:6013–6015. [PubMed: 22576808]
63. Van Vlierberghe S, Dubruel P, Schacht E. Biopolymer-based hydrogels as scaffolds for tissue engineering applications: a review. Biomacromolecules. 2011; 12:1387–1408. [PubMed: 21388145]

64. Ishihara K, Ziats NP, Tierney BP, Nakabayashi N, Anderson JM. Protein adsorption from human plasma is reduced on phospholipid polymers. J Biomed Mater Res. 1991; 25:1397–1407. [PubMed: 1797810]
65. She S, Xu C, Yin X, Tong W, Gao C. Shape deformation and recovery of multilayer microcapsules after being squeezed through a microchannel. Langmuir. 2012; 28:5010–5016. [PubMed: 22381035]
66. Haghgooie R, Toner M, Doyle PS. Squishy Non-Spherical Hydrogel Microparticles. Macromol Rapid Commun. 2010; 31:128–134. [PubMed: 21590884]
67. Cavalieri F, Beretta GL, Cui J, Braunger JA, Yan Y, Richardson JJ, Tinelli S, Folini M, Zaffaroni N, Caruso F. Redox-Sensitive PEG–Polypeptide Nanoporous Particles for Survivin Silencing in Prostate Cancer Cells. Biomacromolecules. 2015; 16:2168–2178. [PubMed: 26120930]
68. Kamaly N, Yameen B, Wu J, Farokhzad OC. Degradable Controlled-Release Polymers and Polymeric Nanoparticles: Mechanisms of Controlling Drug Release. Chem Rev. 2016; 116:2602–2663. [PubMed: 26854975]
69. Haag R, Kratz F. Polymer Therapeutics: Concepts and Applications. Angew Chem Int Ed. 2006; 45:1198–1215.
70. Duffy CV, David L, Crouzier T. Covalently-crosslinked mucin biopolymer hydrogels for sustained drug delivery. Acta Biomater. 2015; 20:51–59. [PubMed: 25818947]
71. Koetting MC, Guido JF, Gupta M, Zhang A, Peppas NA. pH-responsive and enzymatically-responsive hydrogel microparticles for the oral delivery of therapeutic proteins: Effects of protein size, crosslinking density, and hydrogel degradation on protein delivery. J Control Release. 2016; 221:18–25. [PubMed: 26616761]
72. Truong-Le V, Lovalenti PM, Abdul-Fattah AM. Stabilization challenges and formulation strategies associated with oral biologic drug delivery systems. Adv Drug Deliv Rev. 2015; 93:95–108. [PubMed: 26277263]
73. Van Breemen RB, Li Y. Caco-2 cell permeability assays to measure drug absorption. Expert Opin Drug Metab Toxicol. 2005; 1:175–185. [PubMed: 16922635]
74. Renukuntla J, Vadlapudi AD, Patel A, Boddu SH, Mitra AK. Approaches for enhancing oral bioavailability of peptides and proteins. Int J Pharm. 2013; 447:75–93. [PubMed: 23428883]
75. Luo YY, Xiong XY, Tian Y, ZLL, Gong YC, Li YP. A review of biodegradable polymeric systems for oral insulin delivery. Drug Deliv. 2016; 23:1882–1891. [PubMed: 26066036]
76. Castell JV, Jover R, Martnez-Jimnez CP, Gmez-Lechn MJ. Hepatocyte cell lines: their use, scope and limitations in drug metabolism studies. Expert Opin Drug Metab Toxicol. 2006; 2:183–212. [PubMed: 16866607]
77. Rao KM, Rao KK, Ramanjaneyulu G, Ha CS. Curcumin encapsulated pH sensitive gelatin based interpenetrating polymeric network nanogels for anticancer drug delivery. Int J Pharm. 2015; 478:788–795. [PubMed: 25528297]
78. Ravar F, Saadat E, Gholami M, Dehghankelishadi P, Mahdavi M, Azami S, Dorkoosh FA. Hyaluronic acid-coated liposomes for targeted delivery of paclitaxel, in-vitro characterization and in-vivo evaluation. J Control Release. 2016; 229:10–22. [PubMed: 26968799]
79. Banerjee A, Qi J, Gogoi R, Wong J, Mitragotri S. Role of nanoparticle size, shape and surface chemistry in oral drug delivery. J Control Release. 2016; 238:176–185. [PubMed: 27480450]
80. Dasgupta S, Auth T, Gompper G. Shape and Orientation Matter for the Cellular Uptake of Nonspherical Particles. Nano Lett. 2014; 14:687–693. [PubMed: 24383757]
81. He X, Liu F, Yan J, Zhang Y, Yan J, Shang H, Dou Q, Zhao Q, Song Y. Trans-splicing repair of mutant p53 suppresses the growth of hepatocellular carcinoma cells in vitro and in vivo. Sci Rep. 2015; 5:8705. [PubMed: 25732051]
82. Rivlin N, Brosh R, Oren M, Rotter V. Mutations in the p53 Tumor Suppressor Gene: Important Milestones at the Various Steps of Tumorigenesis. Genes Cancer. 2011; 2:466–474. [PubMed: 21779514]
83. Saha MN, Jiang H, Jayakar J, Reece D, Branch DR, Chang H. MDM2 antagonist nutlin plus proteasome inhibitor velcade combination displays a synergistic antimyeloma activity. Cancer Biol Ther. 2010; 9:936–944. [PubMed: 20418664]

Appendix A. Supplementary material

Supplementary material about synthesis procedure of anti-cancer drug BA-TPQ, zeta-potential measurements of PMAA and BA-TPQ-hydrogel cubes, and a confocal image of Nile Red-loaded hydrogel cubes is available from the Elsevier Online Library.

Statement of Significance

Many potent anticancer drugs are hydrophobic and lack tumor selectivity, which limits their application in cancer therapy. Although cubical hydrogels of poly(methacrylic acid) exhibit excellent biocompatibility and versatility, they have not been investigated for hydrophobic drug delivery due to poor mechanical stability and incompatibility between hydrophobic drugs and a hydrophilic hydrogel network. In this study, we provide a facile method to prepare a multilayer hydrogel-based platform with controlled nanostructure, cubical shape and redox-responsiveness for delivery of highly potent anticancer therapeutics, hydrophobic BA-TPQ. The BA-TPQ-hydrogel cubes have exceptional structural stability upon lyophilization which is advantageous for a long-term storage. The greatly enhanced trans-epithelial permeability and amplified anti-tumor activity of BA-TPQ are achieved by encapsulation in these hydrogel cubes. Furthermore, the anticancer BA-TPQ-hydrogel platform retains the selective activity of BA-TPQ to hepatocellular carcinoma cells. Overall, the produced BA-TPQ-hydrogel cubes demonstrate a high potential for clinical liver cancer therapy.

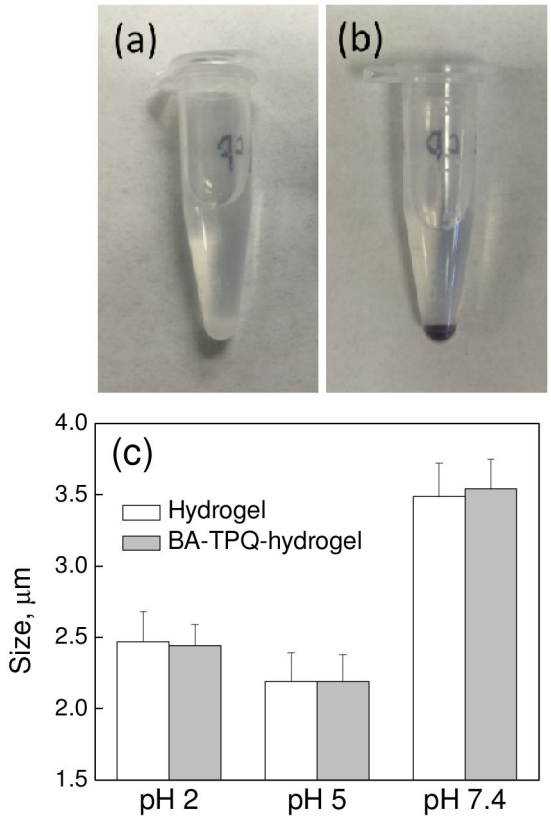

Fig. 1.

Photographs (a, b) of PMAA hydrogel cubes before (a) and after (b) loading with BA-TPQ in 0.01 mM phosphate buffer at pH = 7.4. (c) pH-induced size variations of PMAA hydrogel (white) and BA-TPQ-hydrogel (gray) cubes.

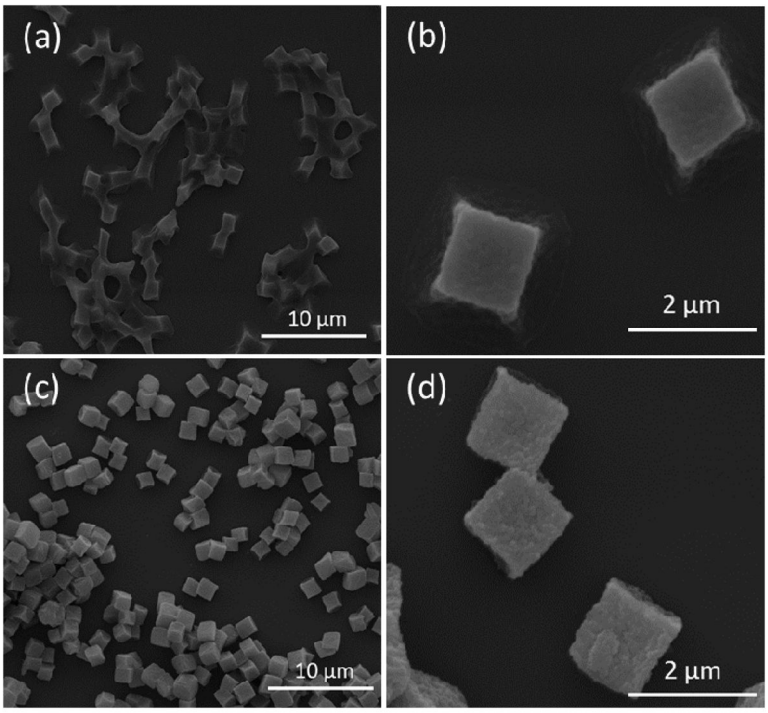

Fig. 2.

SEM images of (a, b) PMAA hydrogel and (c, d) BA-TPQ-hydrogel cubes dried on Si wafer surfaces from solution.

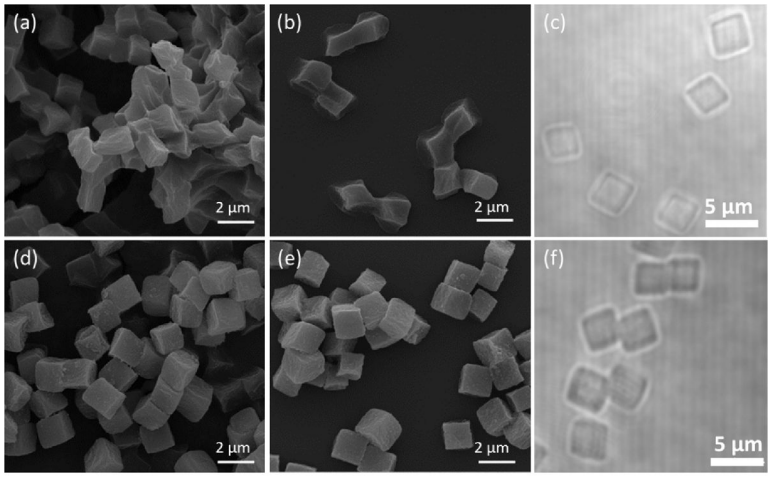

Fig. 3.

SEM images of (a, b) PMAA hydrogel and (d, e) BA-TPQ-hydrogel cubes which were first freeze-dried from solution (a, d) and then re-dispersed in pH = 7.4 buffer and dried again from solution (b, e). Optical microscopy images of re-dispersed (c) PMAA hydrogel and (f) BA-TPQ-hydrogel cubes in pH = 7.4 phosphate buffer.

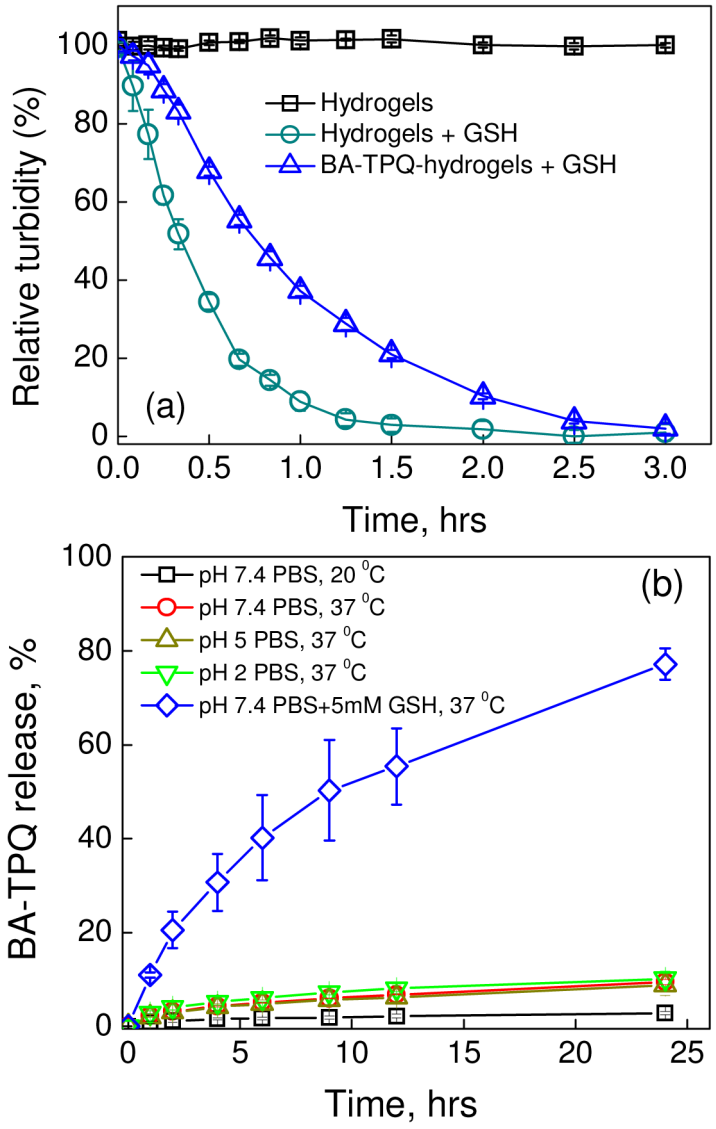

Fig. 4.

(a) Degradation of PMAA hydrogels (hydrogels) and BA-TPQ-hydrogel cubes (BA-TPQ-hydrogels) in the presence of 5mM glutathione (GSH) at pH = 7.4 (PBS, 37 °C) monitored using fluorometry (λ=700 nm). (b) Cumulative release of BA-TPQ (%) from BA-TPQ-hydrogel cubes at 20 °C (pH=7.4), 37 °C (pH =2, 5 or 7.4) and 37 °C in the presence of 5 mM GSH (pH = 7.4) as monitored by UV-vis spectroscopy.

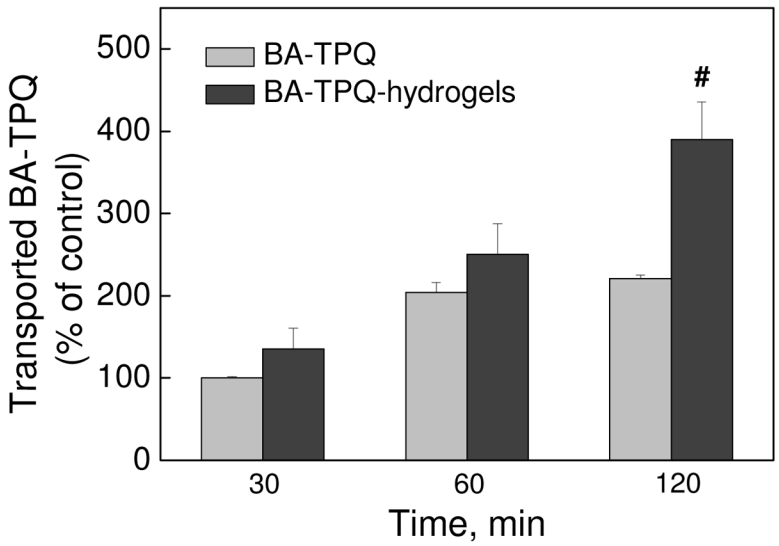

Fig. 5.

In vitro permeability of BA-TPQ, pristine or from BA-TPQ-hydrogels, from apical compartment to the basolateral compartment across Caco-2 cell monolayers at 37 °C as determined by HPLC analysis. The transported BA-TPQ of treatment (BA-TPQ, 5 μg/mL, 30 min) was used as 100% control. All assays were performed in triplicate and were repeated at least three times. The data were analyzed by Student's *t*-test and are shown as the means ± SD. ($^{\#}$ $P < 0.01$)

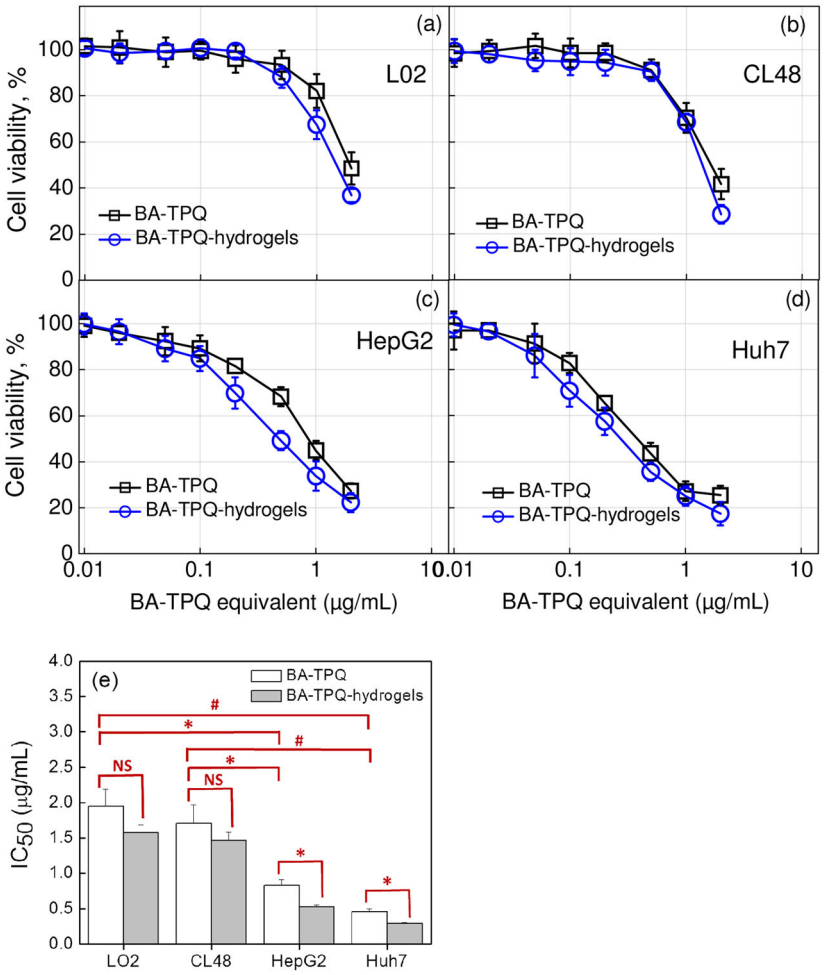

Fig. 6.

(a–d) *In vitro* cytotoxicity of BA-TPQ-hydrogels to LO2, CL48, HepG2, and Huh7 cells. The incubation time is 72 hours. (e) The determined IC_{50} values of BA-TPQ and BA-TPQ-hydrogels. All assays were performed in triplicate and were repeated at least three times. The data were analyzed by Student's *t*-test and are shown as the means ± SD. (* $P < 0.05$, # $P < 0.01$, and "NS" denotes "not significant")

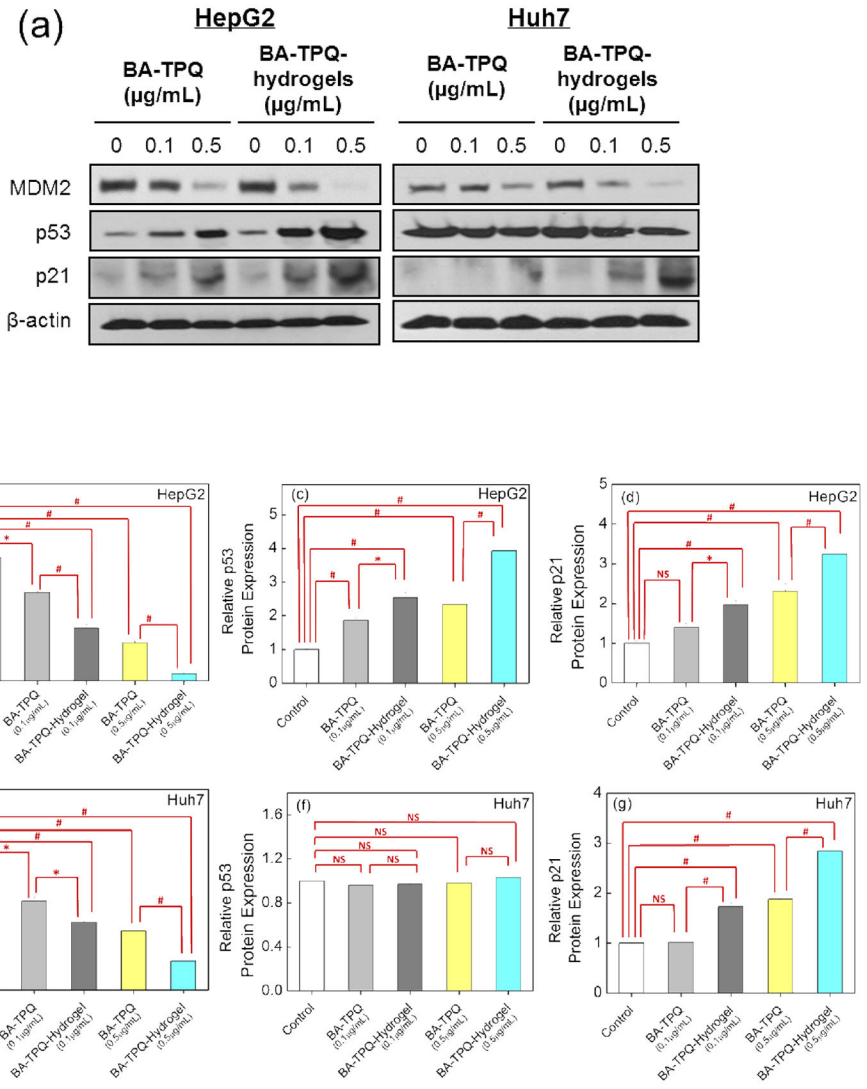

Fig. 7.

(a) The protein expression of MDM2, p53 and p21 in HepG2 and Huh7 cells upon exposure to various concentrations of BA-TPQ and BA-TPQ-hydrogels determined by Western blot. The quantification of protein expression levels in HepG2 (b–d) and Huh7 (e–g) cells was performed using the IMAGE J software with normalization to the untreated control. All assays were repeated at least three times. The data were analyzed by Student's *t*-test and are shown as the means ± SD. (* $P < 0.05$, # $P < 0.01$, and "NS" denotes "not significant")

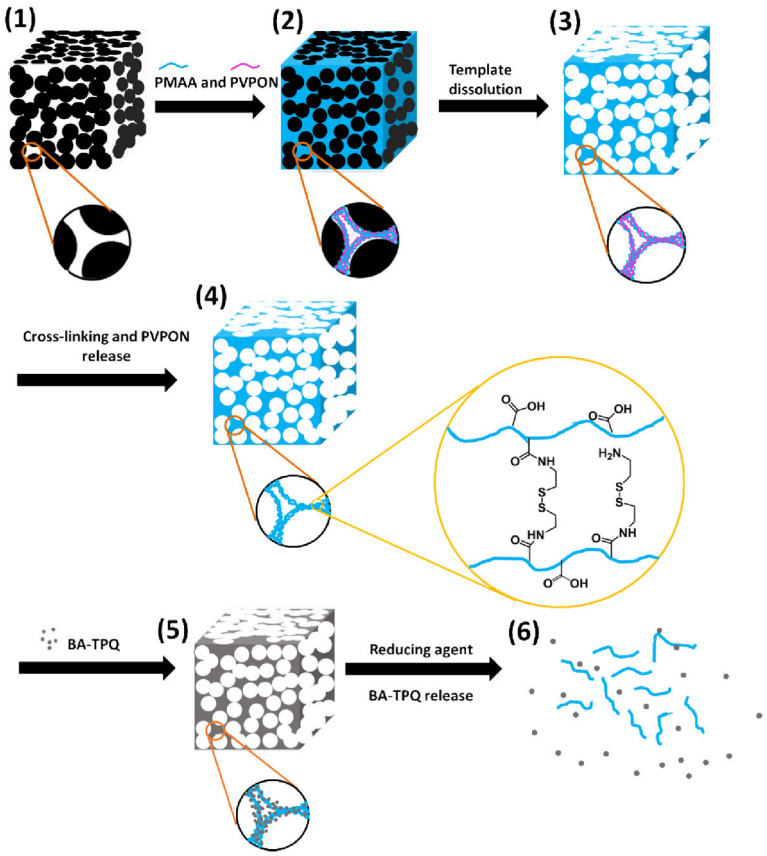

Scheme 1.

Schematic illustration of synthesis, redox-triggered biodegradation and drug release of BA-TPQ-hydrogel cube (BA-TPQ-hydrogel). (1) PEI-coated porous Mn_2O_3 cubic template; (2) Hydrogen-bonded PMAA/PVPON multilayers inside the pores of the template; (3) Hydrogen-bonded PMAA/PVPON multilayers after template dissolution; (4) Cystamine cross-linked PMAA hydrogel cube; (5) Hydrophobic drug (BA-TPQ) encapsulation in PMAA multilayer hydrogel; (6) Redox-triggered degradation of the hydrogel cube and subsequent BA-TPQ release.